Materials Science & Engineering C 123 (2021) 111972

Contents lists available at ScienceDirect

Materials Science & Engineering C

journal homepage: www.elsevier.com/locate/msec

# Enhancing osteoregenerative potential of biphasic calcium phosphates by using bioinspired ZIF8 coating

Mahsa Asadniaye Fardjahromi [a,b], Fatemeh Ejeian [c,d], Amir Razmjou [c,e,f], Graham Vesey [g], Subhas Chandra Mukhopadhyay [a], Amin Derakhshan [d], Majid Ebrahimi Warkiani [b,h,*]

[a] School of Engineering, Macquarie University, Sydney, NSW 2109, Australia
[b] School of Biomedical Engineering, University of Technology Sydney, Sydney, NSW 2007, Australia
[c] Department of Biotechnology, Faculty of Biological Science and Technology, University of Isfahan, Isfahan 73441-81746, Iran
[d] Department of Animal Biotechnology, Reproductive Biomedicine Research Center, Royan Institute for Biotechnology, ACECR, Isfahan, Iran
[e] Centre for Technology in Water and Wastewater, University of Technology Sydney, Sydney, NSW 2007, Australia
[f] UNESCO Centre for Membrane Science and Technology, School of Chemical Engineering, University of New South Wales, Sydney, NSW 2052, Australia
[g] Regeneus Ltd, Paddington, Sydney, NSW, 2021, Australia
[h] Institute of Molecular Medicine, Sechenov First Moscow State University, Moscow 119991, Russia

ARTICLE INFO

*Keywords:*
Osteoinductivity
Zeolitic imidazolate framework-8
Metal organic thin film
Bone regeneration
Alloplastic bone grafts

ABSTRACT

Biphasic calcium phosphate ceramics (BCPs) have been extensively used as a bone graft in dental clinics to reconstruct lost bone in the jaw and peri-implant hard tissue due to their good bone conduction and similar chemical structure to the teeth and bone. However, BCPs are not inherently osteoinductive and need additional modification and treatment to enhance their osteoinductivity. The present study aims to develop an innovative strategy to improve the osteoinductivity of BCPs using unique features of zeolitic imidazolate framework-8 (ZIF8). In this method, commercial BCPs (Osteon II) were pre-coated with a zeolitic imidazolate framework-8/polydopamine/polyethyleneimine (ZIF8/PDA/PEI) layer to form a uniform and compact thin film of ZIF8 on the surface of BCPs. The surface morphology and chemical structure of ZIF8 modified Osteon II (ZIF8-Osteon) were confirmed using various analytical techniques such as XRD, FTIR, SEM, and EDX. We evaluated the effect of ZIF8 coating on cell attachment, growth, and osteogenic differentiation of human adipose-derived mesenchymal stem cells (hADSCs). The results revealed that altering the surface chemistry and topography of Osteon II using ZIF8 can effectively promote cell attachment, proliferation, and bone regeneration in both *in vitro* and *in vivo* conditions. In conclusion, the method applied in this study is simple, low-cost, and time-efficient and can be used as a versatile approach for improving osteoinductivity and osteoconductivity of other types of alloplastic bone grafts.

## 1. Introduction

Bone grafting is a surgical procedure for reconstructing bone defects that may be caused by injuries or trauma, infected nonunions, and genetic disorders [1,2]. Annually over two million bone grafting procedures occur around the world, which makes bone grafts the second most common transplant procedure after the blood transfusion [3,4]. Bone grafts provide support for the progenitor cells to attach, differentiate into bone cell lineage, and grow until new bone tissue forms in defects [5,6]. The gold standard for bone grafting is the autogenous bone graft which is a rich source of cells and growth factors to promote both stem cell recruitment and osteogenic differentiation. However, a limited amount of bone supply and surgical sophistication restrict the use of autogenous bone grafts in clinical cases [7]. After autogenous bone grafts, allografts are considered as an alternative option due to their high osteoinductivity and osteoconductivity. Nonetheless, immunogenic reactions and an increased risk of disease transmission are the biggest challenges when using allografts in bone grafting [8,9]. Another option is to use alloplastic bone grafts which are synthetic materials and can be fabricated on a large scale.

A wide range of substances has been used in the synthesis of alloplastic bone grafts such as metals, polymers, bioactive glasses, and calcium phosphate ceramics (CaPs) [10,11]. Among them, CaPs are gaining greater acceptance in dentistry and medical applications due to their

* Corresponding author at: School of Biomedical Engineering, University Technology Sydney, Sydney, New South Wales, Australia.
*E-mail address:* majid.warkiani@uts.edu.au (M.E. Warkiani).

https://doi.org/10.1016/j.msec.2021.111972
Received 29 October 2020; Received in revised form 31 January 2021; Accepted 10 February 2021
Available online 17 February 2021

desired bioactivity, osteoconductivity, and chemical similarity to the mineral component of teeth and bone [12]. One of the examples of CaPs is biphasic calcium phosphate ceramics (BCPs) which comprises a mixture of different concentrations of hydroxyapatite (HA) and beta-tricalcium phosphate (β-TCP). The optimum concentration of HA in the BCPs can promote cell proliferation and differentiation, and the optimum concentration of β-TCP can control the biosorption and consequently lead to effective bone repair [13,14]. However, BCPs, like other CaPs, suffer from a lack of mechanical stability and osteoinductivity [12,15–21].

A common strategy for enhancing osteoinductivity is using biomolecules (*e.g.*, recombinant human bone morphogenic proteins (rhBMPs)) in the fabrication of bone grafts. BMPs can effectively promote osteoinductivity but increase the risk of inflammation, ectopic bone formation, or cancer [22,23]. In addition, this method is successful in high doses of biomolecules, which makes this strategy cost-inefficient for large scale production of bone grafts [24,25]. Natural biomaterials such as collagen and fibronectin have been applied for bone tissue engineering due to their osteoconductivity and osteoinductivity potential [26]. However, such approaches are unsatisfactory because of poor mechanical strength, batch-to-batch variation, risk of contamination, and allergic reactions caused by natural polymer [27–29]. Thus, synthetic biomaterials with osteoinductive potential are highly desired for the modification of the bone grafts.

A commonly used synthetic biomaterial for the modification of BCPs is calcium phosphate-based materials in which release of calcium and phosphate ions by these materials play a key role in inducing osteogenic differentiation and bone repair. For instance, BCPs are modified with HA using different techniques such as hydrothermal deposition, microwave irradiation, polymer matrix mediated synthesis method, and polymeric sponge methods [13,30–32]. However, long synthesis time, complexity, and heterogeneity of modifications are the main issues that need to be addressed. In addition to CaPs, synthetic materials, including carbon nanotubes, gold nanoparticles, nano glass, and strontium [33–35], have been found useful in the differentiation of stem cells into osteoblast cells. Nonetheless, utilizing conformal thin-film coating instead of nanoparticles is proven to be more effective in generating uniform bone grafts; thus controlling the physicochemical properties of the surface (*e.g.*, wettability, surface area, roughness) and consequently improving the cell attachment and osteogenic differentiation [36]. Among advanced materials such as carbon-based porous structures [37–39] or metal oxides [40,41], metal-organic frameworks (MOFs) has gained great attention. MOFs are nonporous materials comprised of metal clusters of ions linked with organic ligands [42]. These components are linked together by a covalent bond to form an unlimited network structure. The MOF materials have been recently applied in various fields such as energy storage, catalysis, and filtration due to their high porosity, surface area, high chemical and mechanical resistance, and chemical functionality [43–45]. Among different subclasses of MOFs, Zeolitic imidazolate framework-8 (ZIF8) constructed from $Zn^{2+}$ ions and 2-MIM ligands exhibit great potential in biomedical applications on account of their high biocompatibility, pH responsivity, good degradability, and large drug loading capacity [46]. The majority of MOFs either have toxic elements such as chromium [47], or they have non-acquire based synthesis routes, while ZIF8 thin film can be prepared using acquire based methods [48–50]. ZIF8 has been successfully used as carrying therapeutic agents, protecting living cells from external environments, and anti-bactericidal agents [51–54]. Moreover, ZIF8 has been employed as a biomaterial in tissue engineering. We recently introduced the impressive potential of the ZIF8 thin film layer for surface modification of bone scaffolds [56]. The exceptional ability of ZIF8 for enhancing the osteoconductivity and osteoinductivity of scaffolds could be explained by three main reasons. First, ZIF8 modification of scaffolds leads to changing physicochemical properties of the surface, such as hydrophilicity, roughness, functionality, and subsequently enhance cell attachment, growth, and differentiation [55,56]. Second, ZIF8 incorporated scaffolds release Zn elements during scaffold degradation which has been proved to be important in osteoblast differentiation and enhancing bone regeneration [57]. Furthermore, ZIF8 can be applied to load and release bioactive molecules required for osteogenic differentiation due to their high porosity and high specific surface area [58,59]. In addition, ZIF8 as an efficient reinforcement material can be incorporated with synthetic polymers to enhance scaffolds' mechanical properties [57].

We have previously demonstrated that ZIF8 thin-film can modify surface properties of microcarriers and promote stem cell attachment and proliferation in 3D cell culture [60]. Here we employed ZIF8 thin-film coating as a facile method for enhancing osteoinductivity and osteoconductivity of BCPs. In this study, we used Osteon II (Osteon) as one of the commercially available BCPs for periodontal applications with a ratio of 30/70 (HA/BCP). Osteon was modified with polydopamine/polyethyleneimine (PDA/PEI) to mediate *in-situ* crystallization of the ZIF8 thin layer on the surface of Osteon (ZIF8-Osteon) (Fig. 1). Finally, the capability of the ZIF8-Osteon to support cell attachment, proliferation, and osteogenic differentiation were compared with Osteon in both *in vitro* and *in vivo* conditions.

## 2. Experimental

### 2.1. Material

Osteon II (Dentium, Seoul, Korea) was purchased from Minimax implant and dental company, Australia. Dopamine hydrochloride acid, polyethyleneimine (PEI), tris (hydroxymethyl), aminomethane (Tris base), 2-methylimidazole (2-MIM), Zinc nitrate, phalloidin (fluorescein isothiocyanate labeled peptide), and Triton X-100 were purchased from Sigma Aldrich, Australia. Minimum essential medium eagle alpha modification (αMEM), fetal bovine serum (FBS), penicillin/streptomycin, Purelink RNA Mini Kit, Revert Aid First Strand cDNA Synthesis Kit, SYBR Green Master Mix, osteogenic differentiation medium (StemPro™ Osteogenesis Differentiation Kit), and DAPI were purchased from Thermo Fisher Scientific, Australia. MTS Assay Kit, Anti-Collagen 1 antibody (COL-1), Anti-Osteocalcin (OCN), Goat Anti-Mouse (IgG) obtained from Abcam, Australia.

### 2.2. Synthesis of the ZIF8-Osteon

Osteon was coated with ZIF8 thin-film according to the procedure explained elsewhere [60,61]. Briefly, 1 g Osteon was immersed in Tris base buffer (pH 8.5) containing 2 mg/ml DA-HCl and 2 mg/ml PEI. The resulting mixture was shaken gently by an orbital shaker for 16 h. Then PDA coated Osteon (PDA-Osteon) was washed with DI water several times and dried at 40 °C. To fabricate ZIF8 coated Osteon (ZIF8-Osteon), a solution of (Zn $(NO_3)_2$) (2.74 mg/ml) and 2-MIM (56.6 mg/ml) was added to the 1 g PDA-Osteon, and the mixer was left at room temperature. After 2 h, the ZIF8-Osteon was rinsed with DI water and ethanol several times and dried at 40 °C.

### 2.3. Characterization of ZIF8-Osteon

The elemental composition of the ZIF8-Osteon was analyzed using Energy-dispersive X-ray spectroscopy (EDX) (Zeiss Supra 55VP, Zeiss NTS GmbH, Oberkochen, Germany). Attenuated total reflectance-Fourier transform infrared (ATR-FTIR) spectroscopy of the bone grafts were performed using a Thermo Scientific Nicolet 6700ATR spectrophotometer (Thermo Fisher Scientific, Waltham, MA, USA). The powder X-ray diffraction (XRD) profile of Osteon samples was conducted by X-ray diffractometer (D8 Discover XRD, Bruker, USA) for 2θ from 4 to 36° (0.026° step size) with Cu Ka radiation 0.15418 nm.

### 2.4. Cell seeding on bone grafts

Primary human adipose-derived mesenchymal stem cells (hADSCs)

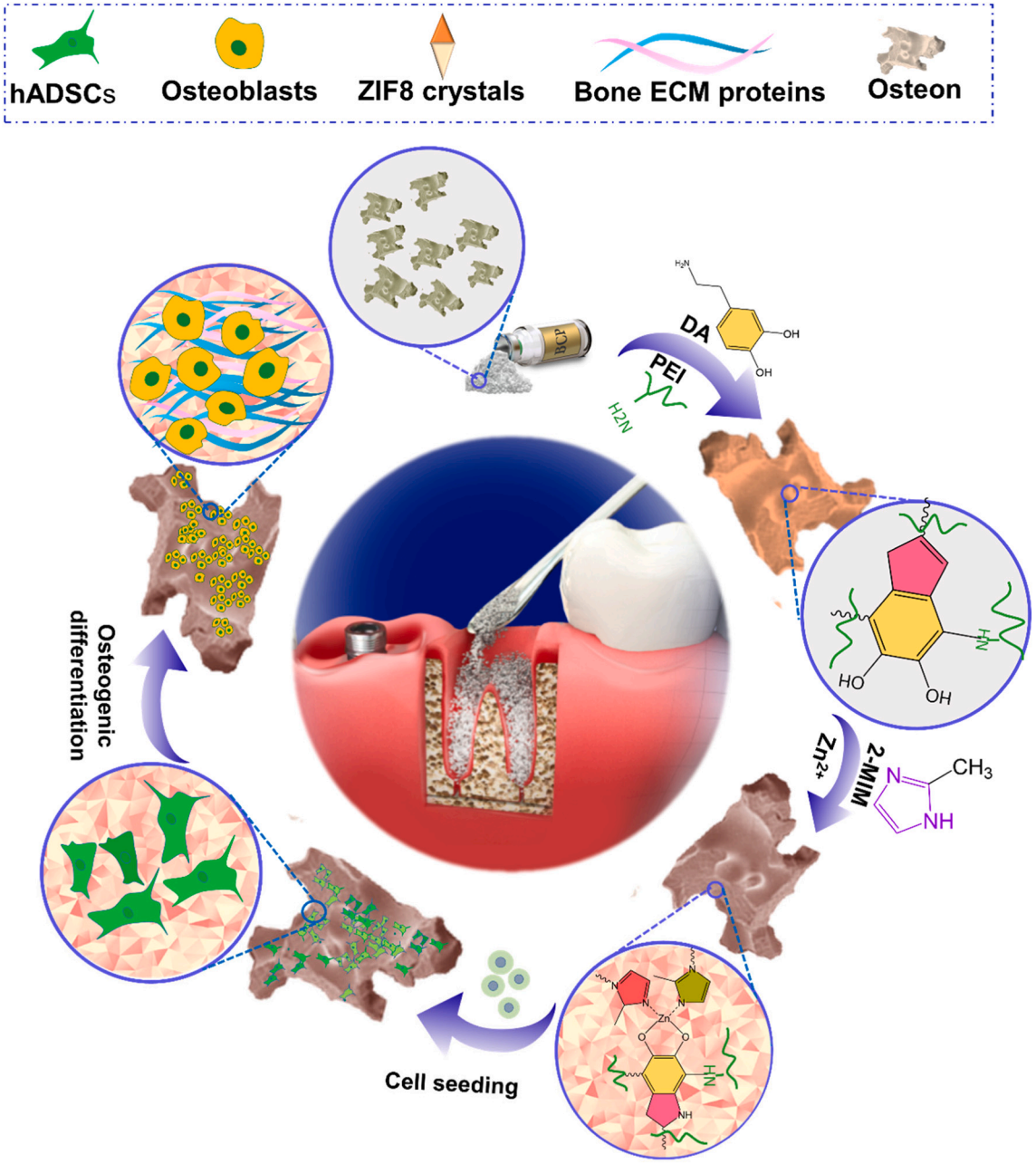


**Fig. 1.** Schematic illustration for the fabrication of the ZIF8-Osteon and improving Osteoinductivity and Osteoconductivity of Osteon for periodontal applications. Briefly, Osteon was immersed on Tris base buffer solution with PEI and DA-HCl and then a solution containing (2-MIM) and $Zn(NO_3)_2$ to form ZIF8 crystals on the surface of Osteon. The fabricated the ZIF8-Osteon was seeded with hADSCs to assess its potential in cell attachment, growth, and new bone formation.

were obtained from Regeneus Ltd, Australia. The cells were maintained in the αMEM medium containing 10% FBS and 1% penicillin/streptomycin. The ZIF8-Osteon was sterilized in ethanol 70% (v/v) followed by UV exposure for 30 min. Prior to the cell seeding, the ZIF8-Osteon was incubated in the culture medium overnight. The hADSCs were seeded on the Osteon and the ZIF8-Osteon with a density of $3.5 \times 10^3$ hADSCs/mg in the ultra-low adherent 24 well plates (Corning) and incubated at 37 °C and 5% $CO_2$ for 7 days.

### 2.5. Confocal microscopy images

To observe cell growth and morphology, samples on the 1st, 3rd, and 7th day of cell culture were rinsed with PBS three times and fixed with 4% (v/v) paraformaldehyde for 30 min. Afterwards, bone grafts were immersed in 0.2% Triton X-100 for 10 min, washed with PBS, and stained with phalloidin. Finally, nuclides were stained with DAPI, and samples were scanned under a confocal microscope (FV3000RS, Olympus, Tokyo, Japan).

### 2.6. Proliferation assay

Cell proliferation of hADSCs cultured on the ZIF8-Osteon and Osteon was assessed using MTS colorimetric assay on the 1st, 3rd, and 7th day of culture according to the kit instruction. The absorbance was recorded at 490 nm by the multimode microplate reader (Tecan Spark, Switzerland).

### 2.7. Cytotoxicity assay

The biocompatibility of the ZIF8-Osteon was assessed by MTS colorimetric assay. The bone grafts were sterilized with 70% ethanol and

ultraviolet radiation for 1 h. Afterwards, the samples were placed into a 24-well plate and immersed with αMEM media with 10% FBS and incubated at 37 °C for 24 h to obtain the extract solution. At the same time, hADSCs were cultured at 96-well plate with a density of $5 \times 10^4$ cell/ml at 37 °C in a humidified atmosphere containing 5% $CO_2$ to allow cell attachment. After 24 h, the culture medium was removed, and the extract solution was added to the well plate. Finally, the viability of the samples was quantified using MTS assay after 24 and 72 h incubation and reading absorbance at 490 nm according to the following equation:

$$\text{Viable cells } (\%) = \left(\text{Absorbance}_{\text{sample}} - \text{Absorbance}_{\text{blank}}\right) / \left(\text{Absorbance}_{\text{negative control}} - \text{Absorbance}_{\text{blank}}\right) \times 100$$

### 2.8. Scanning electron microscopy (SEM)

Bone grafts after 7 days of culture were washed with DPBS, and the cells were fixed in 2.5% glutaraldehyde for1 h. Next, they were dehydrated with a series of ethanol from 30% to 100% and air-dried. Samples were sputter-coated with gold-palladium with a thickness of 15 nm (EM ACE600, Leica, Germany). Bone grafts without cells were directly sputter-coated with gold-palladium. All the bone grafts were visualized with a Zeiss Supra 55VP microscope.

### 2.9. Osteogenic differentiation

The hADSCs were cultured on bone grafts in αMEM medium, including 10% FBS and 1% penicillin/streptomycin. 3 days after cell seeding, the medium was replaced with osteogenic differentiation medium, and the medium was refreshed every 3 days. The plate was maintained at 37 °C in a humidified atmosphere containing 5% $CO_2$ incubator for 21 days.

### 2.10. Immunofluorescence

After 21 days of osteogenic induction, bone grafts were washed with PBS. Cells were fixed with 4% paraformaldehyde for 20 min and were permeabilized using 1% Triton X-100. The samples were washed with PBS three times and then incubated with COL-1 and OCN overnight at 4 °C. After washing with PBS three times, samples were incubated with FITC-conjugated secondary antibody for 1 h at room temperature and observed with confocal microscope (FV3000RS, Olympus, Tokyo, Japan). The mean fluorescent intensity (MIF) was calculated using the ImageJ software from three independent experiments.

### 2.11. Alizarin Red S quantification

Alizarin Red S staining was used to identify the presence of extracellular matrix calcium deposits after 21 days of osteogenic differentiation. Briefly, cells treated with osteogenic differentiation media were fixed in ethanol for 15 min and stained with an aqueous solution containing 0.2% Alizarin Red S adjusted in pH 4.2 at room temperature for 1 h. For the quantitative analysis of staining, bone grafts were immersed in an aqueous solution containing 20% methanol and 10% acetic acid for 15 min. The liquid was then read at a wavelength of 450 nm by using a Spark multimode microplate reader.

### 2.12. Real time-PCR

In order to evaluate the efficiency of differentiation, the expression of some bone-specific markers (*ALP*, *BMP2*, *SPP1*) was quantified using qRT-PCR. After 21 days of induction, total RNA was extracted using Pure Link RNA Mini Kit and reverse-transcribed into cDNA by using Revert Aid First Strand cDNA Synthesis Kit, according to the manufacturer's instructions. Subsequently, the qRT-PCR analysis was performed using SYBR™ Green Master Mix on a Thermal Cycler Bio-Rad CFX96 (Bio-Rad, USA) under optimal reaction condition as follow: 95 °C for 10 min, followed by 40 cycles of 95 °C for 10 s, 60 °C for 1 min and 72 °C for 10 s temperature. Target gene expressions were normalized to *ACTB* housekeeping gene and calculated based on the ddCt method. The primer sequence of genes designed for real time-PCR is summarized in Table 1.

### 2.13. Surgical procedure

This study was performed on four adult male New Zealand rabbits (weight: 2.5–3.0 kg) following approval from the Ethics Committee for experimental animals, Royan Institute (IR.ACECR.ROYAN.REC.1397.21), and in accordance with the Animal Research: Reporting *In vivo* (ARRIVE) guidelines [62]. Prior to surgery, rabbits were adapted under standard conditions for seven days in individual cages. The general anaesthesia was induced by intramuscular injection using a combination of 40 mg/kg ketamine hydrochloride (10% Ketamine, Alfasan, Netherlands, Woerden) and 5 mg/kg xylazine (2% Xylazine, Alfasan, Netherlands, Woerden). The scalp was disinfected and shaved, and calvarial bone was exposed *via* a full-thickness midline incision. Subsequently, under saline irrigation, three circular defects (2 mm depth/8 mm diameter) were created around the sagittal suture using a trephine bur. Two out of three defects were filled with 0.5 mg of Osteon or the ZIF8-Osteon, while the control defect kept unfilled. To minimize the uncontrollable effect of the implant site, materials were placed in a clockwise direction for individual rabbits, according to a modified Latin square design. Lastly, the soft tissues were closed using 3/0 silk sutures, and the animals received antibiotics (penicillin, 400,000 U/d) for 3 days. At the end of four weeks after surgery, the animals were euthanized by an overdose of intravenous injection of pentobarbital (100 mg/kg IV). The surgical area of calvarial bones was dissected out, and the X-ray radiographs were taken using X-ray radiography (Siemens, Germany, Munich) for analyzing bone tissue regeneration, with 55 kV irradiation for 12 s and 80 cm distance from the target. The density of new bone tissues was quantified for all groups applying Image J software (Version 1.42q, National Institutes of Health, USA).

**Table 1**
Primer sequences of the genes used for the real-time PCR.

| Gene | Sequence | Gene ID |
|---|---|---|
| *COL1A* | Forward 5′-TAGTCTGTCCTGCGTCCTCTG-3′<br>Reverse 5′-TTTTGCTTCCTCCCACCCCTA-3′ | 1277 |
| *SPP1* | Forward 5′-TTCGCAGACCTGACATCCA-3′<br>Reverse 5′-CCATTCAACTCCTCGCTTTCC-3′ | 6696 |
| *ALPL* | Forward 5′-CTGATGTGGAGTATGAGAGT-3′<br>Reverse 5′-AGTGGGAGTGCTTGTATC-3′ | 249 |
| *BMP2* | Forward 5′-TAGCAGTTTCCATCACCGAA-3′<br>Reverse 5′-CACTTCCACCACGAATCCATG-3′ | 650 |

### 2.14. Histological analysis

The harvested specimens from each group were fixed with 0.5% formaldehyde and then decalcified by 10% EDTA at 4 °C for 5 weeks. Afterwards, the sample blocks were dehydrated in a graded alcohol series, embedded in paraffin, and perpendicular sections (6-μm thickness) were prepared along the central region of defects. Sections were stained with hematoxylin and eosin (H&E) and visualized by light microscopy (Olympus, BX51, Japan). New bone formation was measured in three randomly selected fields using Image-Pro Plus software. Moreover, the probable inflammatory response was analyzed by evaluating the presence of inflammatory cells in the analyzed area.

### 2.15. Statistical analysis

The statistical significance of the differences between the experimental groups was determined using the Student's *t*-test method using Graph Pad Prism7 software. Significance levels were shown as *p < 0.05, **p < 0.01, ***p < 0.001, and ****p < 0.0001.

## 3. Results

### 3.1. Characterization

The ZIF8-Osteon was fabricated by coating Osteon with PDA and forming Zinc chelation through catechol groups on the surface of PDA-Osteon. Fig. 2A–C shows the change in colour of Osteon from white to brown after coating with PDA and PDA-ZIF8. The surface morphology of Osteon before and after coating with PDA and ZIF8 were investigated with SEM. Fig. 2A indicates the surface of HAP/β-TCP ceramics in the Osteon is clean, and the crystals are exhibiting elongated hexagonal bipyramid shapes with a grain size of 1–3 μm. After PDA/PEI coating in the basic condition, a polydopamine film was formed on the surface of Osteon (Fig. 2B). Following ZIF8 *in situ* crystallization, a dense ZIF8 crystal layer is formed on the surface of Osteon (Fig. 2C). ZIF8 formation was examined by EDX (Fig. 2D). The presence of Zinc atoms after coating the ZIF8 layer on the surface of Osteon confirms the formation of ZIF8 on the surface of Osteon. The FT-IR spectrum of Osteon indicates peaks at 1022, 969, and 550 $cm^{-1}$ corresponding to $PO_4^{3-}$groups at BCPs. In the FTIR spectrum of PDA-Osteon, the peaks at 1646 $cm^{-1}$ assign the C═N bonds during the formation of imine by the Schiff base reaction between PDA and PEI, and the peaks at 1450, 1375 indicates C═C stretching. FTIR spectrum of the ZIF8-Osteon reveals a peak at 429 $cm^{-1}$ which is associated with Zn—N stretching in tetrahedrally coordinated $Zn^{2+}$ with 2-MIM ligands. The formation of ZIF8 was confirmed by the XRD analysis. The XRD pattern of the ZIF8-Osteon shows major characteristic peaks of ZIF8 at $2\theta = 7.45, 10.86, 12.9, 14.83$ which are in great agreement with simulated ZIF8 XRD patterns [63].

### 3.2. Cell attachment and proliferation

To investigate the cell attachment, spreading, and proliferation of hADSCs on the surface of Osteon and the ZIF8-Osteon, the cell nucleus and actin filaments were stained with DAPI and phalloidin, respectively. The confocal microscopy images revealed that in the first 24 h, the number of cells adhered to the surface of the ZIF8-Osteon was more than

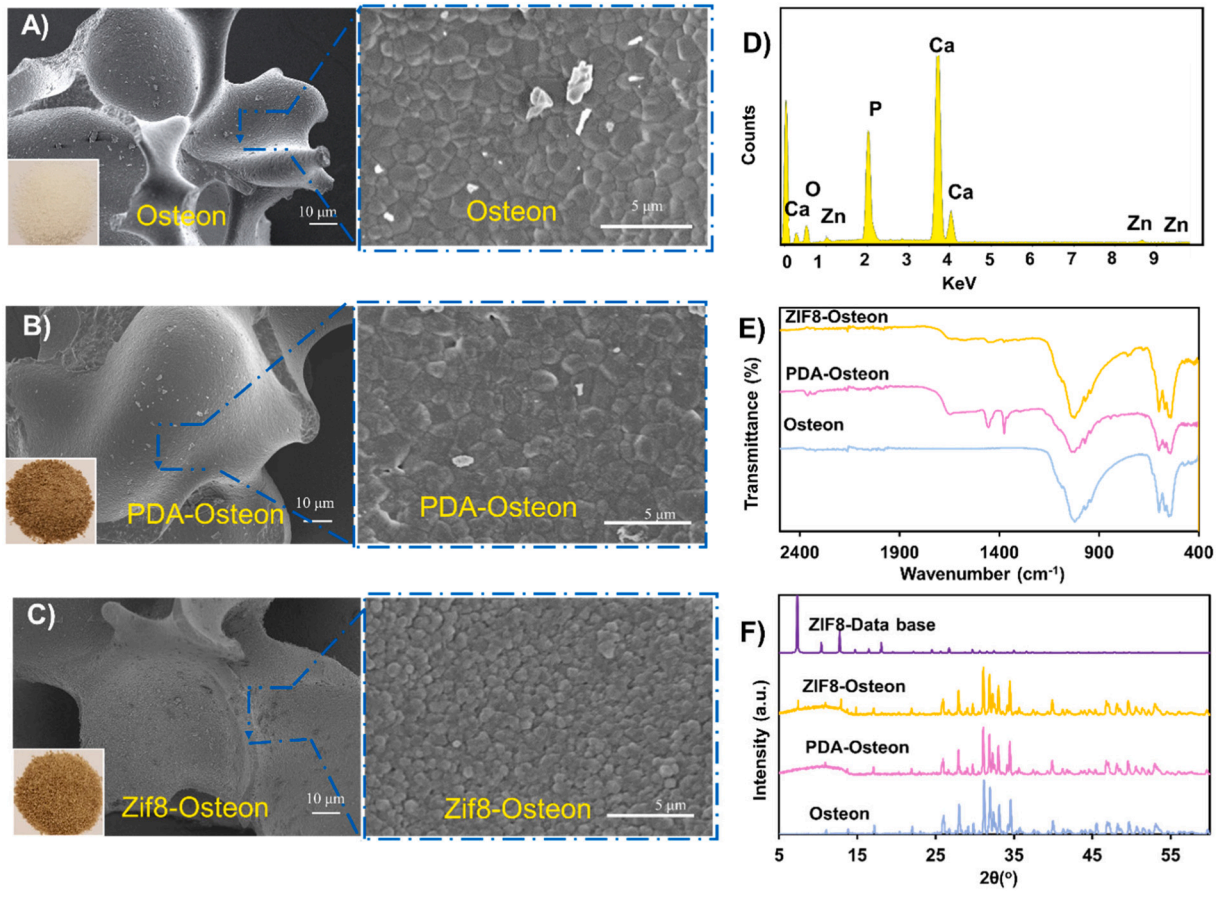


**Fig. 2.** Characterization of morphology and structure of bone grafts. SEM and digital images of Osteon (A), PDA-Osteon (B), and the ZIF8-Osteon (C). The color of Osteon changed from white to brown after coating with PDA/PEI and ZIF/PDA/PEI. A dense ZIF8 crystal layer formed on the surface of Osteon by coating ZIF8/PDA/PEI. SEM-EDX spectra of the ZIF8-Osteon (D). FTIR-ATR spectrum of Osteon after coating with PDA and ZIF8 (E). XRD spectra of Osteon coated with PDA/PEI and ZIF/PDA/PEI (F). (For interpretation of the references to color in this figure legend, the reader is referred to the web version of this article.)

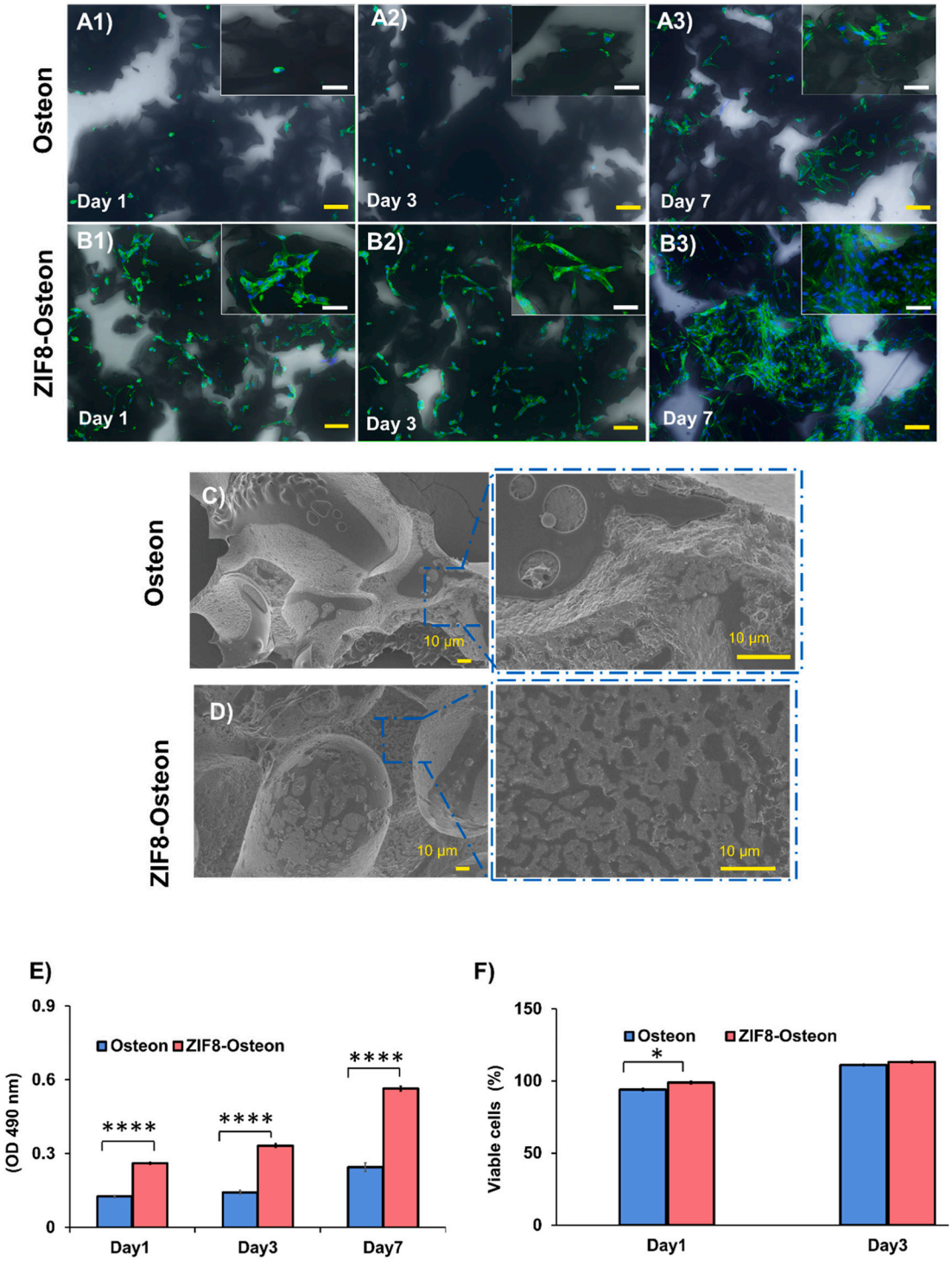


**Fig. 3.** Comparison of hADSCs attachment and proliferation on the surface of Osteon before and after coating with ZIF8. DAPI/phalloidin staining after 1, 3, and 7 days of culturing on the surface of Osteon (A1-A3) and the ZIF8-Osteon (B1-B3) indicate cell attachment and growth enhanced by coating ZIF8 crystals. F-actin filaments were visualized *via* FITC labeled phalloidin (green) and nuclides with DAPI (blue). Yellow scale bars indicate100 µm, and white scale bars indicate 50 µm. SEM images of cells attached to Osteon (C) and the ZIF8-Osteon (D) after 7 days of culture show more cell growth on the surface of Osteon-ZIF8 compared with Osteon. MTS viability/proliferation of Osteon and the ZIF8-Osteon (E). MTS cytotoxicity assay of hADSCs in contact with extraction media exposed to Osteon and ZIF8-Osteon after 1 and 3 days of incubation (F). Data are presented as mean ± SEM (****p value $< 0.0001$, n $\geq 3$). (For interpretation of the references to color in this figure legend, the reader is referred to the web version of this article.)

Osteon alone with a higher cell spreading area, normal spindle-shaped, and flat morphology (Fig. 3A1 and B1). Over time, ADSCs maintained their morphology and continued to expand until a dense cell layer was formed on the surface of the ZIF8-Osteon on 7$^{th}$ day of culture (Fig. 3B2 and B3). On the contrary, the adhered cells on the surface of Osteon had rounded shapes on day 1, and moderate cell expansion was observed on day 3 onwards. Overall, these results suggest a small number of cells could grow on the surface of Osteon (Fig. 3A1–A3). The cell morphology and cell proliferation of the ZIF8-Osteon were evaluated by SEM microscopy, too (Fig. 3C and D). SEM images confirmed a greater number of hADSCs covered the ZIF8-Osteon, suggesting the ZIF8 layer can potentially enhance the cell adhesion and support higher cell growth.

Cell viability of hADSCs on ZIF8 coated substrates was assessed by the MTS assay (*i.e.*, through measurement of the cell metabolic activity). Fig. 3E indicates ZIF8 modification did not have any cytotoxic effect. In contrast, cells cultured on the ZIF8-Osteon even proliferated at a faster rate and reached a significantly higher level of metabolic activity compared with the Osteon alone.

### 3.3. Cytotoxicity

The cytotoxicity of ZIF8-Osteon was assessed *in vitro* by using MTS assay against hADSCs. The viability of cells cultured in the extraction medium exposed to Osteon was used as a control. Fig. 3F revealed that ZIF8-Osteon has a significantly higher viability rate when compared with the control (Osteon) after 24 h incubation. On day 3 the viability

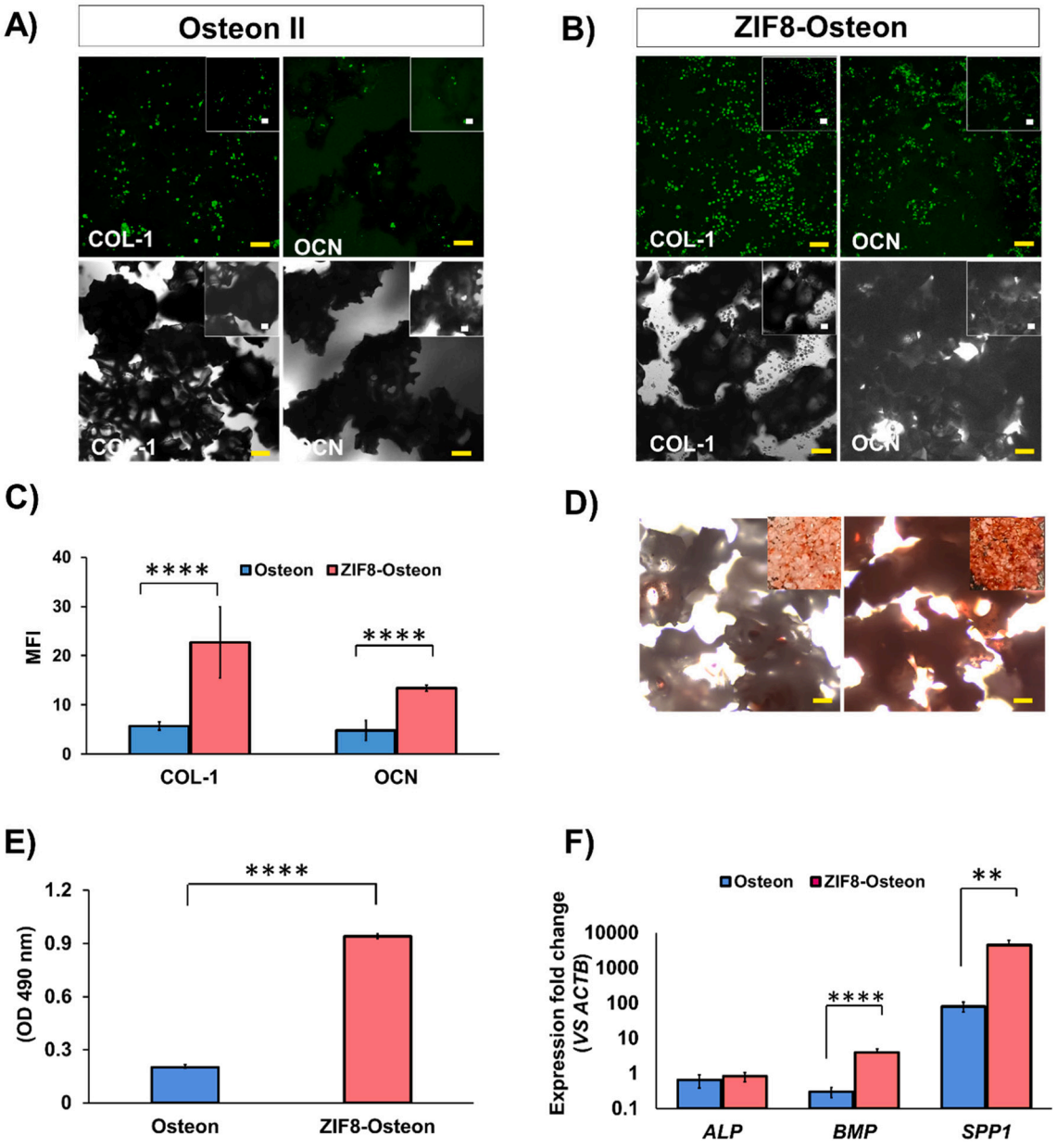


**Fig. 4.** Evaluation of ZIF8 coating in osteogenic differentiation of hADSCs: Expression of osteogenic markers (COL-1 and OCN) in hADSCs cultured on Osteon (A) and the ZIF8-Osteon (B) after 3 weeks of treatment with osteogenic supplements. Mean fluorescent intensity analyzed with ImageJ (C). High expression of COL-1 and OCN secreted from hADSCs was observed in the ZIF8-Osteon. Yellow scale bars and white scale bars indicate100 μm and 50 μm, respectively. Alizarin Red S staining for Osteon (left panel) and ZIF8- Osteon (right panel) (D). Alizarin Red S quantification of Osteon and the ZIF8-Osteon (E). The ZIF8-Osteon exhibited a higher extent of mineralization than Osteon; Real-time RT-PCR analysis of genes involved in osteogenesis (F). Data are represented as mean ± SEM, from four independent experiments. (**p value $< 0.01$, and****p value $< 0.0001$, n $\geq$ 3). (For interpretation of the references to color in this figure legend, the reader is referred to the web version of this article.)

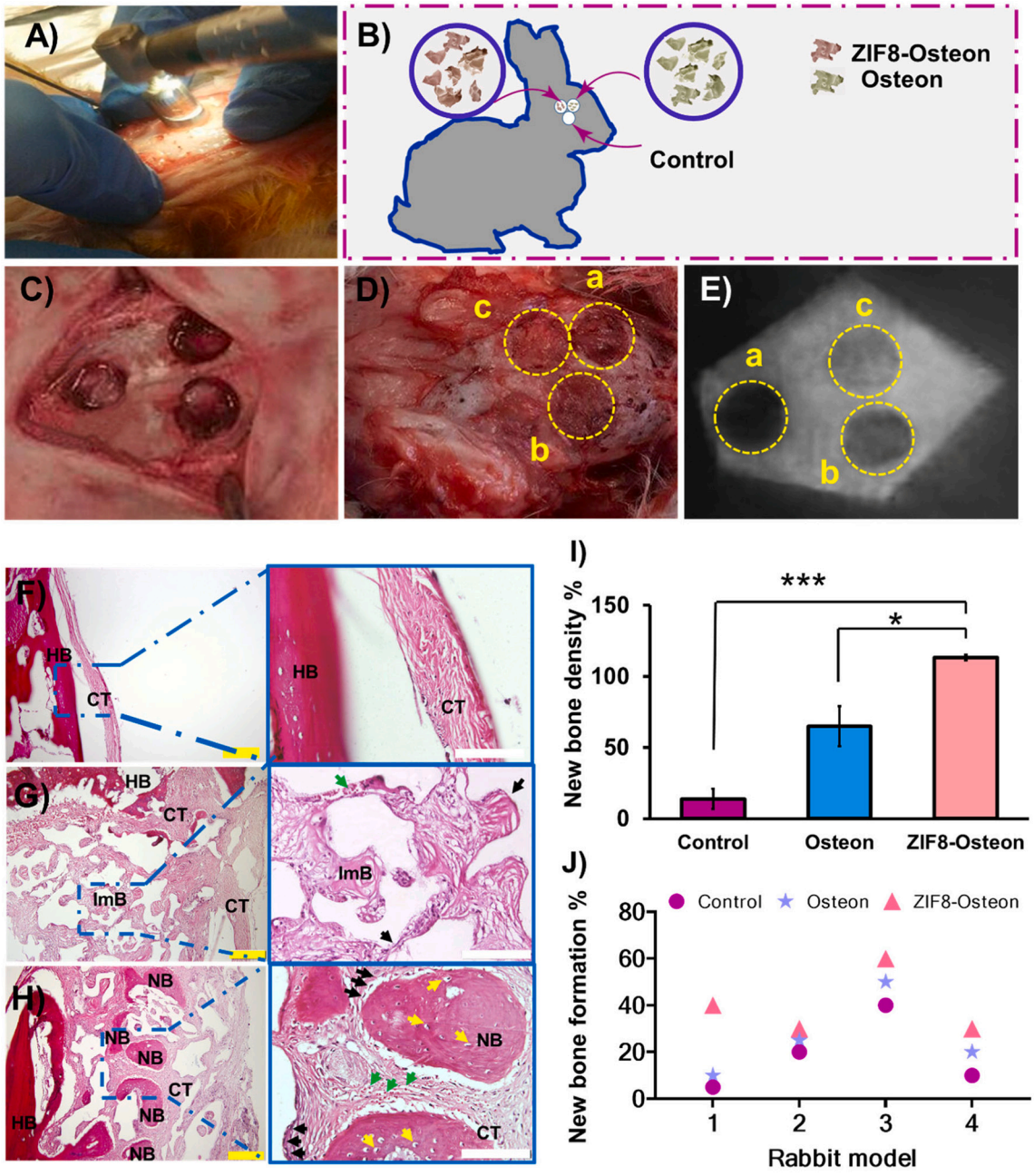


**Fig. 5.** *In vivo* bone regeneration in a rabbit calvarial defect model: Surgical presentation of bone defect formation using a trephine bur and continuous saline irrigation at the surgical site (A). Schematic of *in vivo* experimental setup (B). Osteon and the ZIF8-Osteon were implanted on two of the defects, and one defect remains unfilled as a control. Image of defects with a diameter of 8 mm created on the parietal bone of rabbits (C). Macroscopic view (D) and X-ray graph of a representative rabbit model four weeks after post-surgery (E). a: Control, b: Osteon, and c: The ZIF8-Osteon groups. Histological images of H&E stained bone sections after four weeks' post-surgery in Control (F), Osteon (G), and the ZIF8-Osteon (H). After four weeks of healing, significant higher new bone formation was observed in the ZIF8-Osteon compared with Osteon and control group. New bone formation, host bone tissue, immature bone tissue, and connective tissue are shown by NB, HB, ImB, and CT, respectively. Black arrows indicate lining osteoblasts, yellow arrows show osteocytes trapped in lacuna, and green arrows mark blood cells. Yellow scale bars indicate 200 μm, and white scale bars indicate 100 μm. Quantitative analysis of micro-CT images displayed significantly higher bone density in the ZIF8-Osteon (*p value $< 0.05$, and ***p value $< 0.001$, $n = 4$) (I). Individual percentage value of new bone formation in experimental groups for four rabbit models (J). (For interpretation of the references to color in this figure legend, the reader is referred to the web version of this article.)

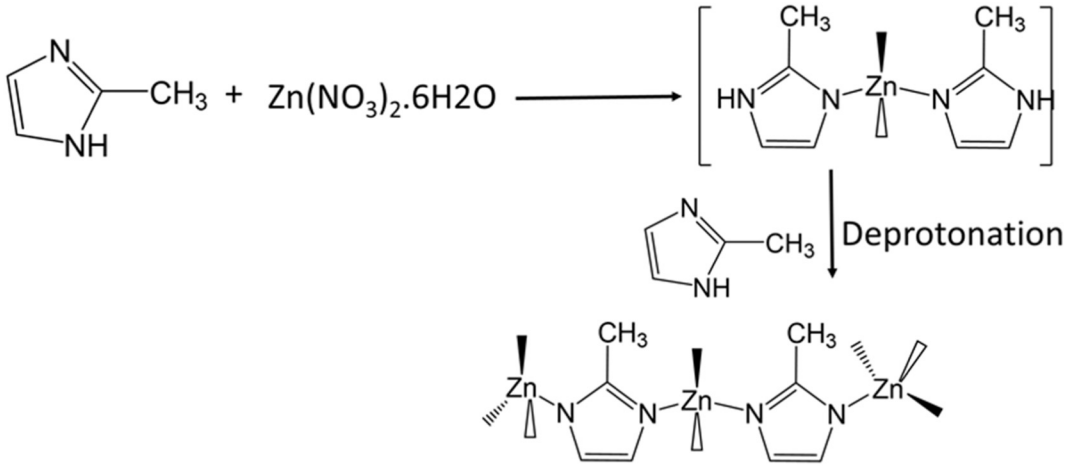


**Fig. 6.** A plausible mechanism for the formation of ZIF-8 crystals on the surface of PDA-PEI.

rate value raised more than 100% which indicates ZIF8 coating does not have any cytotoxicity effect and enhances cell proliferation.

### 3.4. Osteogenic differentiation

The osteogenic potential of the ZIF8-Osteon and Osteon were evaluated with immunofluorescence staining of hADSCs with *COL-1* and *OCN* as typical bone-specific markers. The confocal microscopy images of hADSCs attached to the ZIF8-Osteon indicated a high expression level of *COL-1* and *OCN*. However, weak green fluorescence was observed for the cells differentiated on the surface of Osteon alone, reflecting a lower expression of *COL-1* and *OCN* proteins (Fig. 4A and B). In addition to that, the quantification of fluorescent intensity in Fig. 4C indicates that *COL-1* and *OCN* expression in ZIF-Osteon increased significantly compared with Osteon. Calcium mineralization was detected by staining bone grafts with Alizarin Red S after 21 days of osteoinduction. The scanned image of mineralization presents more intense red staining (Fig. 4D) and significantly higher calcification ability of the ZIF8-Osteon in comparison with naked Osteon (Fig. 4E).

Further osteogenic differentiation potential of ZIF8 modification was performed through the mRNA expression of a series of osteogenic genes such as *ALP*, *BMP2*, and *SPP* as the specific markers of early, middle, and late stages of osteogenesis, respectively. Fig. 4F shows a slight increase in *ALP* expression of the ZIF8-Osteon which suggests ZIF8 coating did not have a significant effect on the early osteogenic differentiation of hADSCs against Osteon. On the contrary, significantly higher levels of *BMP2* and *SPP* expression were observed in cells seeded on the ZIF8-Osteon which demonstrates that ZIF8 modification enhances the later osteogenic differentiation potential of hADSCs.

### 3.5. In vivo bone regeneration

The bone regeneration capacity of Osteon and the ZIF8-Osteon bone substituents was assessed in a rabbit calvarial defect model (Fig. 5A–C). All animals recovered well, and no signs of infection or inflammation were detected during the follow-up period. After four weeks of implantation, the macroscopic analysis revealed newly formed bone tissues at the defect sites implanted with the Osteon and the ZIF-Osteon composite. However, maximum osseous regeneration was observed with defects filled with the ZIF8-Osteon (Fig. 5D). The radiographic densitometry images and quantitive analysis also verified significantly higher bone density in the ZIF8-Osteon-grafted defects compared to other groups (a 2-fold increase relative to the Osteon and a 9-fold increase When compared with the control) (Fig. 5E, I). Histological evaluation of bone regeneration revealed the formation of loose connective tissue (CT) in the border area of host bone tissue (HB) in the control group and generation of new immature woven bone tissue (ImB) on the Osteon defect site (Fig. 5F and G). Meanwhile, in the ZIF8-Osteon group, a new trabecular bone (NB) matrix contained mature osteocytes were formed in the defect area (Fig. 5H). In addition, higher vascularized connective tissue and bone-lining osteoblast was observed in the ZIF8-Osteon compared with other groups. The result of histomorphometric analysis in four rabbit models is summarized in Fig. 5J, which confirmed the higher level of new bone formation in the ZIF8-Osteon group in all animals.

## 4. Discussion

The high osteoconductivity of BCPs makes them a suitable material for bone grafts in maxillo-facial and orthopedic surgeries [64]. However, limited osteoinductivity of BCP ceramics poses a limit in their applications in regenerative medicine. While many studies have focused on using biomolecules for enhancing the osteoinductivity of BCPs, the purpose of this study was to explore the efficacy of ZIF8 thin-film coating to enhance the osteoconductivity of BCPs.

The first step toward modification of BCPs is to ensure the ZIF8 thin-film is biocompatible and does not mask their bioactivity and osteoconductivity. The results of cytoskeletal staining by phalloidin and MTS assay confirmed cells are healthy and maintained their morphology on the surface of the ZIF8-Osteon. A comparison of cell attachment and proliferation of the ZIF8-Osteon and Osteon alone showed that the ZIF8 coating does not reduce the bioactivity of Osteon and improves cell attachment and proliferation significantly. Our findings suggest that ZIF8 coating can enhance better the cell attachment and proliferation of BCPs compare to the traditional coating techniques using synthetic polymers such as poly(lactic-*co*-glycolic acid) (PLGA), poly(D, L-lactic acid) (PDLLA), and polycaprolactone (PCL) [65–69]. According to the literature, several factors such as roughens, composition, porosity, surface charge, surface energy, and functional groups can impact cell adhesion to BCPs [70]. Our technique for modification of BCPs shows a clear change in the surface morphology of Osteon, generating rough nanotopography compared to the smooth surface of naked Osteon. This has been observed for other surfaces such as silicon and tissue culture plates using the AFM analysis [60,71]. Our previous study also confirmed that ZIF8 coating can increase wettability and surface free energy, resulting in better cell attachment and growth [60].

The present study demonstrated that the ZIF8-Osteon has a higher osteogenic differentiation capacity and produce more intracellular mineralization than Osteon alone (Fig. 4). These results have further strengthened our confidence in using ZIF8 modification as a method to improve the osteogenic potential of BCPs. In fact, the osteoinductivity of Osteon modified by ZIF8 is as high as BCPs immobilized by biomolecules

and growth factors *in vitro* and *in vivo* conditions reported in previous works [72–75]. The high osteoinductive potential of the ZIF8-Osteon is in line with previous results which confirmed bone grafts incorporated with Zn ions can significantly favour osteogenic differentiation through releasing $Zn^{2+}$ ions [57,58,76]. In addition to that, the modification of BCPs with ZIF8 as a material with a high surface area can increase the possibility of cell recruitment and adsorption of environmental proteins and growth factors on BCPs. According to Zhue et al., BPSs with porous structures and high surface area play a significant role in the adsorption of proteins and, as a result, promote the osteoinductive potential of BCPs [77]. Lin et al. stated that the surface area of bioceramics increases with hierarchical 3D micro-nanotextured. This higher surface area enhances the capability of ceramics in Vitronectin and Fibronectin protein adsorption and consequently improves the osteogenic differentiation potential of cells [78]. Taken together, our *in vitro* results are in agreement with the *in vivo* findings, which displayed a reasonable degree of regeneration of compact bone tissues in the ZIF8-Osteon transplanted defects after a relatively short time. However, the formation of immature bony tissues in the presence of Osteon grafts was observed in defect edges.

Some studies have shown that modification of BCPs with nanomaterials can enhance the osteoinductivity of BCPs. In fact, a bone matrix is composed of two phases: organic components that contain many proteins such as collagen, fibronectin, and inorganic part, includes HA and $Ca_{10}(PO_4)_6(OH)_2$. Both these phases are at the nanoscale, so bone grafts with nanostructure can exhibit better interaction with bone tissue and affect their functionality [79]. For example, Hu et al. showed nano-HA coating using the hydrothermal deposition method could promote osteoconductivity and osteoinductivity of BCP significantly [80]. In the present study, ZIF8 modification formed compact nanocrystals on the surface of Osteon which could well be responsible for stimulating osteogenic differentiation.

The method presented in this study for modification of BCPs showed a homogenous coating of ZIF8 on the surface of Osteon (Fig. 2). In fact, uniform modification of Osteon is closely associated with using PDA and PEI in the fabrication of the ZIF8-Osteon. The interacting PDA with PEI through covalent bond assists in forming uniform PDA coating on the surface of Osteon. In fact, ZIF8 crystals were formed on the surface of PDA-PEI in a water-based system at room temperature, and the formed PDA layer acts as a reducing and stabilizing agent for facilitating nucleation and growth of ZIF8 crystals. The formation of ZIF8 crystals involves the coordination of $Zn^{2+}$ centers with 2-MIM, deprotonation of 2-MIM, and eventually, the formation of ZIF8 crystals, according to Fig. 6 [81]. In contrast, cooperating osteoinductive material during the sintering process or modification using thermal deposition resulted in a non-homogeneous coating [68,78,80]. In addition, the catechol and amino groups on a PDA layer acts as a covalent linker, which allows ZIF8 to adhere tightly to the surface and improve the mechanical stability of the ZIF8 coating [60]. By contrast, modification of BCPs with osteoinductive HA particles using various techniques (*e.g.*, sol-gel coating, thermal spraying, sputter coating, electrophoretic deposition, dip-coating) results in poor mechanical stability of BCPs due to the poor coating–substrate adherence and the brittle property of HA [82].

## 5. Conclusion

We successfully developed an effective approach to enhance the osteoinductivity of BCPs *via* ZIF8 thin-film modification. We demonstrated that the Osteon coated with ZIF8 thin-film exhibits better cell spreading, attachment, and proliferation than uncoated Osteon. In addition, ZIF8 thin-film coating enhances the osteoinduction potential of BCPs significantly which we confirmed by immunostaining, Alizarin Red S staining, and real time-PCR. The results from *in vivo* studies indicate higher new bone formation after 4 weeks of bone healing. The modification of BCPs using this method is time and cost-effective and can be simply performed in mild conditions without using organic solvents or toxic reagents. Overall, this study presents a versatile method for enhancing osteoinductivity and osteoconductivity of BCPs, whereby this method can be extended to other alloplastic bone grafts and help to solve their low osteoinduction potential in bone tissue engineering.

## Data availability

The raw/processed data required to reproduce these findings cannot be shared at this time as the data also forms part of an ongoing study.

## CRediT authorship contribution statement

Conception and design of study: M. Warkiani, M.Asadniaye Fardjahromi, F.Ejeian

Acquisition of data: M.Asadniaye Fardjahromi, F.Ejeian, A. Derakhshan

Analysis and/or interpretation of data: M.Asadniaye Fardjahromi, F. Ejeian, M. Warkiani

Drafting the manuscript: M.Asadniaye Fardjahromi, F.Ejeian

Revising the manuscript critically for important intellectual content: M.Warkaini, A. Razmjou, G. Vesey, S. Mukhopadhyay

Approval of the version of the manuscript to be published (the names of all authors must be listed):

Mahsa Asadniaye Fardjahromi, Fatemeh Ejeian, Amir Razmjou, Graham Vesey, Subhas Chandra Mukhopadhyay, Amin Derakhshan, Majid Ebrahimi Warkiani

## Declaration of competing interest

The authors declare that they have no known competing financial interests or personal relationships that could have appeared to influence the work reported in this paper.

## Acknowledgements

M.E.W. would like to acknowledge the support of the Australian Research Council through Discovery Project Grants (DP170103704 and DP180103003) and the National Health and Medical Research Council (Australia) through the Career Development Fellowship (APP1143377). We also acknowledge Regeneus (Australia) for generous funding of this research.

## References

[1] P.N. Mittwede, R. Gottardi, P.G. Alexander, I.S. Tarkin, R.S. Tuan, Clinical applications of bone tissue engineering in orthopedic trauma, Curr Pathobiol Rep 6 (2) (2018) 99–108.
[2] A. Wiese, H.C. Pape, Bone defects caused by high-energy injuries, bone loss, infected nonunions, and nonunions, Orthop Clin North Am 41 (1) (2010) 1–4.
[3] V. Campana, G. Milano, E. Pagano, M. Barba, C. Cicione, G. Salonna, W. Lattanzi, G. Logroscino, Bone substitutes in orthopaedic surgery: from basic science to clinical practice, J Mater Sci Mater Med 25(10) (2014) 2445–61.
[4] H.S. Cha, J.W. Kim, J.H. Hwang, K.M. Ahn, Frequency of bone graft in implant surgery, Maxillofac Plast Reconstr Surg 38 (1) (2016) 19.
[5] L. Kumar Meena, H. Rather, D. Kedaria, R.J. Vasita, Polymeric microgels for bone tissue engineering applications—a review, Int. J. Polym. Mater. 69 (6) (2020) 381–397.
[6] S. Dutta, D. Passi, P. Singh, A.J Bhuibhar, Ceramic, and non-ceramic hydroxyapatite as a bone graft material: a brief review, Ir. J. Med. Sci. 184 (1) (2015) 101–106.
[7] P. Baldwin, D.J. Li, D.A. Auston, H.S. Mir, R.S. Yoon, K.J. Koval, Autograft, allograft, and bone graft substitutes: clinical evidence and indications for use in the setting of orthopaedic trauma surgery, J. Orthop. Trauma 33 (4) (2019) 203–213.
[8] R. Zamborsky, A. Svec, M. Bohac, M. Kilian, M.J. Kokavec, Infection in bone allograft transplants, Exp. Clin. Transplant. 14 (5) (2016) 484–490.
[9] A.A. Jahangir, R.M. Nunley, S. Mehta, A.J. Sharan, Bone-graft substitutes in orthopaedic surgery, AAos now 2 (1) (2008) 35–37.
[10] D.C. Lobb, B.R. DeGeorge Jr., A. Chhabra, Bone graft substitutes: current concepts and future expectations, J Hand Surg Am 44 (6) (2019) 497–505.
[11] H. Tavassoli, J. Javadpour, M. Taheri, M. Mehrjou, N. Koushki, F. Arianpour, M. Majidi, J. Izadi-Mobarakeh, B. Negahdari, P. Chan, M. Ebrahimi Warkiani, S. Bonakdar, Incorporation of nanoalumina improves mechanical properties and

osteogenesis of hydroxyapatite bioceramics, ACS Biomater Sci Eng 4 (4) (2018) 1324–1336.
[12] J.S. Al-Sanabani, A.A. Madfa, F.A Al-Sanabani, Application of calcium phosphate materials in dentistry, Int. J. Biomater. (2013) 2013 876132.
[13] J. Hu, Z. Yang, Y. Zhou, Y. Liu, K. Li, H. Lu, Porous biphasic calcium phosphate ceramics coated with nano-hydroxyapatite and seeded with mesenchymal stem cells for reconstruction of radius segmental defects in rabbits, J Mater Sci Mater Med 26 (11) (2015) 257.
[14] J.M. Bouler, P. Pilet, O. Gauthier, E. Verron, Biphasic calcium phosphate ceramics for bone reconstruction: a review of biological response, Acta Biomater. 53 (2017) 1–12.
[15] J. Zhang, W. Liu, V. Schnitzler, F. Tancret, J.M. Bouler, Calcium phosphate cements for bone substitution: chemistry, handling and mechanical properties, Acta Biomater. 10(3) (2014) 1035–49.
[16] S. Saber-Samandari, S. Baradaran, B. Nasiri-Tabrizi, K. Alamara, W.J. Basirun, Microstructural evolution and micromechanical properties of thermally sprayed hydroxyapatite coating, Adv. Appl. Ceram. 117 (8) (2018) 452–460.
[17] F. Ghadami, S. Saber-Samandari, G. Rouhi, M. Amani Hamedani, M.M. Dehghan, S. Farzad Mohajeri, F. Mashhadi-Abbas, H. Gholami, The effects of bone implants' coating mechanical properties on osseointegration: in vivo, in vitro, and histological investigations, J. Biomed. Mater. Res. 106(10) (2018) 2679–2691.
[18] S. Saber-Samandari, K.A. Gross c. technology, Nanoindentation on the surface of thermally sprayed coatings, Surf, Coat. Technol 203 (23) (2009) 3516–3520.
[19] S. Saber-Samandari, K.A. Gross, C. Technology, Nanoindentation reveals mechanical properties within thermally sprayed hydroxyapatite coatings, Surf, Coat. Technol 203 (12) (2009) 1660–1664.
[20] K.A. Gross, S. Saber-Samandari, C. Technology, Revealing mechanical properties of a suspension plasma sprayed coating with nanoindentation, Surf, Coat. Technol 203 (2009) 2995–2999.
[21] K.A. Gross, S. Saber-Samandari, K.S. Heemann, Evaluation of commercial implants with nanoindentation defines future development needs for hydroxyapatite coatings, J Biomed Mater Res B 93 (1) (2010) 1–8.
[22] A.W. James, G. LaChaud, J. Shen, G. Asatrian, V. Nguyen, X. Zhang, K. Ting, C. Soo, A review of the clinical side effects of bone morphogenetic protein-2, Tissue Eng Part B Rev 22(4) (2016) 284–97.
[23] E.J. Carragee, G. Chu, R. Rohatgi, E.L. Hurwitz, B.K. Weiner, S.T. Yoon, G. Comer, B. Kopjar, Cancer risk after use of recombinant bone morphogenetic protein-2 for spinal arthrodesis, JBJS 95 (17) (2013) 1537–1545.
[24] P.M. Arrabal, R. Visser, L. Santos-Ruiz, J. Becerra, M. Cifuentes, Osteogenic molecules for clinical applications: improving the BMP-collagen system, Biol, Res. 46 (4) (2013) 421–429.
[25] H. Tavassoli, S.N. Alhosseini, A. Tay, P.P. Chan, S. Oh, M.E. Warkiani, Large-scale production of stem cells utilizing microcarriers: a biomaterials engineering perspective from academic research to commercialized products, Biomaterials 181 (2018) 333–346.
[26] X. Lin, S. Patil, H. Li, D.-x. Wei, G. Yong-Guang, A.J. Qian, The bone extracellular matrix in bone formation and regeneration, Front. Pharmacol. 11 (2020) 455.
[27] T. Adachi, M. Tomita, K. Shimizu, S. Ogawa, K. Yoshizato, Generation of hybrid transgenic silkworms that express Bombyx mori prolyl-hydroxylase α-subunits and human collagens in posterior silk glands: production of cocoons that contained collagens with hydroxylated proline residues, J. Biotechnol.126 (2) (2006) 205–219.
[28] S. Hinderer, S.L. Layland, K. Schenke-Layland, ECM and ECM-like materials—biomaterials for applications in regenerative medicine and cancer therapy, Adv, Drug Deliv. Rev. 97 (2016) 260–269.
[29] A. Garg, S. Garg, M. Kumar, S. Kumar, A.K. Shukla, S. Kaushik, Applications of natural polymers in mucoadhesive drug delivery: an overview, Adv. Pharm. J. 3 (2) (2018) 38–42.
[30] E.G. Pasand, A. Nemati, M. Solati-Hashjin, K. Arzani, A. Farzadi, Materials Metallurgy, Microwave assisted synthesis & properties of nano HA-TCP biphasic calcium phosphate, J. Miner. Metall. Mater.19 (5) (2012) 441–445.
[31] A. Sinha, T. Mishra, N. Ravishankar, Polymer assisted hydroxyapatite microspheres suitable for biomedical application, J Mater Sci Mater Med 19 (5) (2008) 2009–2013.
[32] H.R. Ramay, M. Zhang, Preparation of porous hydroxyapatite scaffolds by combination of the gel-casting and polymer sponge methods, Biomaterials 24 (19) (2003) 3293–3302.
[33] W.C. Lee, C.H. Lim, H. Shi, L.A. Tang, Y. Wang, C.T. Lim, K.P. Loh, Origin of enhanced stem cell growth and differentiation on graphene and graphene oxide, ACS Nano 5(9) (2011) 7334–41.
[34] M. Ribeiro, M.H. Fernandes, M.M. Beppu, F.J. Monteiro, M.P. Ferraz, Silk fibroin/nanohydroxyapatite hydrogels for promoted bioactivity and osteoblastic proliferation and differentiation of human bone marrow stromal cells, Mater Sci Eng C 89 (2018) 336–345.
[35] P. Wang, L. Zhao, J. Liu, M.D. Weir, X. Zhou, H. Xu, Bone tissue engineering via nanostructured calcium phosphate biomaterials and stem cells, Bone Res. 2 (2014) 14017.
[36] M. Mozafari, A. Ramedani, Y. Zhang, D. Mills, Thin Films for Tissue Engineering Applications, Thin Film Coatings for Biomaterials and Biomedical Applications, Woodhead Publishing, 2016, pp. 167–195.
[37] H. Karimi-Maleh, M. Alizadeh, Y. Orooji, F. Karimi, M. Baghayeri, J. Rouhi, S. Tajik, H. Beitollahi, S. Agarwal, V.K. Gupta, S. Rajendran, S. Rostamnia, L. Fu, F. Saberi-Movahed, S. Malekmohammadi, Guanine-based DNA biosensor amplified with Pt/SWCNTs nanocomposite as analytical tool for nanomolar determination of daunorubicin as an anticancer drug: a docking/experimental investigation, Ind, Eng. Chem. Res. 60 (2) (2021) 816–823.
[38] H. Karimi-Maleh, M. Shafieizadeh, M.A. Taher, F. Opoku, E.M. Kiarii, P.P. Govender, S. Ranjbari, M. Rezapour, Y. Orooji, J. Mol. Liq. 298 (2020) 112040.
[39] H. Ziari, A. Habibnejad Korayem, M. Hajiloo, M. Nakhaei, A. Razmjou, H. Divandari, Evaluating the effect of amorphous carbon powder on moisture susceptibility and mechanical resistance of asphalt mixtures, Constra Build Mater. 152 (2017) 182–191.
[40] M. Asadnia, A. Kottapalli, J. Miao, A. Randles, A. Sabbagh, P. Kropelnicki, J. Tsai, High temperature characterization of PZT (0.52/0.48) thin-film pressure sensors, JMM 24(1) (2013) 015017.
[41] H. Karimi-Maleh, B.G. Kumar, S. Rajendran, J. Qin, S. Vadivel, D. Durgalakshmi, F. Gracia, M. Soto-Moscoso, Y. Orooji, F. Karimi, Tuning of metal oxides photocatalytic performance using Ag nanoparticles integration, J. Mol. Liq. 314 (2020) 113588.
[42] Y.-R. Lee, J. Kim, W. Ahn, Synthesis of metal-organic frameworks: a mini review, Korean J. Chem. Eng. 30 (9) (2013) 1667–1680.
[43] A. Ahmed, S. Seth, J. Purewal, A.G. Wong-Foy, M. Veenstra, A.J. Matzger, D. J. Siegel, Exceptional hydrogen storage achieved by screening nearly half a million metal-organic frameworks, Nat. Commun. 10 (1) (2019) 1–9.
[44] L. Zhu, X.-Q. Liu, H.-L. Jiang, L.B. Sun, Metal–organic frameworks for heterogeneous basic catalysis, Chem. Rev. 117 (12) (2017) 8129–8176.
[45] M. Kadhom, B. Deng, Metal-organic frameworks (MOFs) in water filtration membranes for desalination and other applications, Appl. Mater. Today 11 (2018) 219–230.
[46] W. Guan, Y. Dai, C. Dong, X. Yang, Y. Xi, Zeolite imidazolate framework (ZIF)-based mixed matrix membranes for CO2 separation: a review, J. Appl. Polym. Sci. 137 (33) (2020) 48968.
[47] H. Karimi-Maleh, Y. Orooji, A. Ayati, S. Qanbari, B. Tanhaei, F. Karimi, M. Alizadeh, J. Rouhi, L. Fu, M. Sillanpää, Recent advances in removal techniques of Cr(VI) toxic ion from aqueous solution: a comprehensive review, J. Mol. Liq. (2020) 115062.
[48] M. Mohammad, M. Lisiecki, K. Liang, A. Razmjou, V. Chen, Metal-phenolic network and metal-organic framework composite membrane for lithium ion extraction, Appl. Mater. Today 21 (2020) 100884.
[49] S. Zhand, A. Razmjou, S. Azadi, S.R. Bazaz, J. Shrestha, M.A. Jahromi, M. E. Warkiani, Metal-organic framework-enhanced ELISA platform for ultrasensitive detection of PD-L1, ACS Applied Bio Materials 3 (7) (2020) 4148–4158.
[50] M. Nankali, Z. Einalou, M. Asadnia, A. Razmjou, High-sensitivity 3D ZIF-8/PDA photonic crystal-based biosensor for blood component recognition, ACS Applied Bio Materials 4 (2) (2021) 1958–1968.
[51] R. Ettlinger, N. Moreno, D. Volkmer, K. Kerl, H.J. Bunzen, Zeolitic imidazolate framework-8 as pH-sensitive nanocarrier for "arsenic trioxide", drug delivery, Chem. Eur. J. 25 (57) (2019) 13189–13196.
[52] R. Riccò, W. Liang, S. Li, J. Gassensmith, F. Caruso, C. Doonan, P. Falcaro, Metal–organic frameworks for cell and virus biology: a perspective, ACS nano12 (1) (2018) 13–23.
[53] G. Wyszogrodzka, B. Marszalek, B. Gil, P. Dorozynski, Metal-organic frameworks: mechanisms of antibacterial action and potential applications, Drug Discov. Today 21(6) (2016) 1009–18.
[54] S. Keskin, S.J. Kızılel, E.C. Research, Biomedical applications of metal organic frameworks, Ind, Eng. Chem. Res. 50 (4) (2011) 1799–1812.
[55] X. Zhang, J. Chen, X. Pei, J. Wang, Q. Wan, S. Jiang, C. Huang, X. Pei, Enhanced osseointegration of porous titanium modified with zeolitic imidazolate framework-8, ACS Appl. Mater. Interfaces 9 (30) (2017) 25171–25183.
[56] F. Ejeian, A. Razmjou, M.H. Nasr-Esfahani, M. Mohammad, F. Karamali, M. Ebrahimi Warkiani, M. Asadnia, V. Chen, ZIF-8 modified polypropylene membrane: a biomimetic cell culture platform with a view to the improvement of guided bone regeneration, Int. J. Nanomedicine 15 (2020) 10029–10043.
[57] Y. Yang, J. Zan, W. Yang, F. Qi, C. He, S. Huang, S. Peng, C. Shuai, Metal organic frameworks as a compatible reinforcement in a biopolymer bone scaffold, Mater. Chem. Front 4 (3) (2020) 973–984.
[58] B. Tao, W. Zhao, C. Lin, Z. Yuan, Y. He, L. Lu, M. Chen, Y. Ding, Y. Yang, Z.J. Xia, Surface modification of titanium implants by ZIF-8@ Levo/LBL coating for inhibition of bacterial-associated infection and enhancement of in vivo osseointegration, Mater. Chem. Front 390 (2020) 124621.
[59] Ö. Toprak, B. Topuz, Y. Abou Monsef, Ç. Oto, K. Orhan, A.J. Karakeçili, E. C, bmp-6 carrying metal organic framework-embedded in bioresorbable electrospun fibers for enhanced bone regeneration 120, 2020, p. 111738.
[60] M.A. Fardjahromi, A. Razmjou, G. Vesey, F. Ejeian, B. Banerjee, S. C. Mukhopadhyay, M.E.J.R.A. Warkiani, Mussel inspired ZIF8 microcarriers: a new approach for large-scale production of stem cells, RSC Adv. 10 (34) (2020) 20118–20128.
[61] P. Moazzam, H. Tavassoli, A. Razmjou, M.E. Warkiani, M. Asadnia, Mist harvesting using bioinspired polydopamine coating and microfabrication technology, Desalination 429 (2018) 111–118.
[62] J. McGrath, G. Drummond, E. McLachlan, C. Kilkenny, C. Wainwright, Guidelines for reporting experiments involving animals: the ARRIVE guidelines, Br. J. Pharmacol. 160 (7) (2010) 1573–1576.
[63] W. Wong-Ng, J. Kaduk, L. Espinal, M. Suchomel, A. Allen, H. Wu, High-resolution synchrotron X-ray powder diffraction study of bis (2-methylimidazolyl)-zinc, $C_8H_{10}N_4Zn$ (ZIF-8), Powder Diffraction 26(3) (2011) 234–237.
[64] J. Jeong, J.H. Kim, J.H. Shim, N.S. Hwang, C.Y. Heo, Bioactive calcium phosphate materials and applications in bone regeneration, Biomater Res 23 (1) (2019) 4.
[65] X. Miao, D.M. Tan, J. Li, Y. Xiao, R. Crawford, Mechanical and biological properties of hydroxyapatite/tricalcium phosphate scaffolds coated with poly(lactic-co-glycolic acid), Acta Biomater. 4(3) (2008) 638–45.

[66] X. Zhao, Y. Han, J. Li, B. Cai, H. Gao, W. Feng, S. Li, J. Liu, D. Li, BMP-2 immobilized PLGA/hydroxyapatite fibrous scaffold via polydopamine stimulates osteoblast growth, Mater. Sci. Eng. C Mater. Biol. Appl. 78 (2017) 658–666.
[67] C.M. Andreasen, S.S. Henriksen, M. Ding, N. Theilgaard, T.L. Andersen, S. Overgaard, The efficacy of poly-d,l-lactic acid- and hyaluronic acid-coated bone substitutes on implant fixation in sheep, J Orthop Translat 8 (2017) 12–19.
[68] S.I. Roohani-Esfahani, S. Nouri-Khorasani, Z.F. Lu, R.C. Appleyard, H. Zreiqat, Effects of bioactive glass nanoparticles on the mechanical and biological behavior of composite coated scaffolds, Acta Biomater. 7(3) (2011) 1307–18.
[69] C. Shi, Z. Yuan, F. Han, C. Zhu, B. Li, Polymeric biomaterials for bone regeneration 1 (2016) 27.
[70] E.A. dos Santos, M. Farina, G.A. Soares, K. Anselme, Surface energy of hydroxyapatite and beta-tricalcium phosphate ceramics driving serum protein adsorption and osteoblast adhesion, J Mater Sci Mater Med 19(6) (2008) 2307–16.
[71] A. Razmjou, M. Asadnia, O. Ghaebi, H.-C. Yang, M. Ebrahimi Warkiani, J. Hou, V. J. Chen, interfaces, Preparation of iridescent 2D photonic crystals by using a mussel-inspired spatial patterning of ZIF-8 with potential applications in optical switch and chemical sensor, ACS Appl. Mater. 9 (43) (2017) 38076–38080.
[72] J.C. Roldan, R. Detsch, S. Schaefer, E. Chang, M. Kelantan, W. Waiss, T.E. Reichert, G.C. Gurtner, U. Deisinger, Bone formation and degradation of a highly porous biphasic calcium phosphate ceramic in presence of BMP-7, VEGF and mesenchymal stem cells in an ectopic mouse model, J. Craniomaxillofac. Surg. 38(6) (2010) 423–30.
[73] J.W. Jang, J.H. Yun, K.I. Lee, J.W. Jang, U.W. Jung, C.S. Kim, S.H. Choi, K.S. Cho, Osteoinductive activity of biphasic calcium phosphate with different rhBMP-2 doses in rats, Oral Surg. Oral Med. Oral Pathol. Oral Radiol. 113(4) (2012) 480–7.
[74] J. Baek, H.-D. Jung, T.-S. Jang, S.W. Kim, M.-H. Kang, H.-E. Kim, Y. Koh, Synthesis and evaluation of bone morphogenetic protein (BMP)-loaded hydroxyapatite microspheres for enhanced bone regeneration, Ceram. Int. 42 (6) (2016) 7748–7756.
[75] B.-R. Kim, T. Nguyen, Y.-K. Min, B. Lee, In vitro and in vivo studies of BMP-2-loaded PCL–gelatin–BCP electrospun scaffolds, Tissue Eng, Part A 20 (23–24) (2014) 3279–3289.
[76] G. Wang, S.I. Roohani-Esfahani, W. Zhang, K. Lv, G. Yang, X. Ding, D. Zou, D. Cui, H. Zreiqat, X. Jiang, Effects of Sr-HT-gahnite on osteogenesis and angiogenesis by adipose derived stem cells for critical-sized calvarial defect repair, Sci. Rep. 7(1) (2017) 41135.
[77] X. Zhu, H. Fan, Y. Xiao, D. Li, H. Zhang, T. Luxbacher, X. Zhang, Effect of surface structure on protein adsorption to biphasic calcium-phosphate ceramics in vitro and in vivo, Acta Biomater. 5 (4) (2009) 1311–1318.
[78] K. Lin, L. Xia, J. Gan, Z. Zhang, H. Chen, X. Jiang, J.J.A.a.m. Chang, interfaces, Tailoring the nanostructured surfaces of hydroxyapatite bioceramics to promote protein adsorption, osteoblast growth, and osteogenic differentiation, ACS Appl. Mater. Interfaces 5(16) (2013) 8008–8017.
[79] H. Yi, F.U. Rehman, C. Zhao, B. Liu, N. He, Recent advances in nano scaffolds for bone repair, Bone Res. 4 (1) (2016) 1–11.
[80] J. Hu, Y. Zhou, L. Huang, J. Liu, H. Lu, Effect of nano-hydroxyapatite coating on the osteoinductivity of porous biphasic calcium phosphate ceramics, BMC Musculoskelet. Disord. 15 (1) (2014) 114.
[81] M. Jian, B. Liu, R. Liu, J. Qu, H. Wang, X. Zhang, Water-based synthesis of zeolitic imidazolate framework-8 with high morphology level at room temperature, RSC Adv. 5 (60) (2015) 48433–48441.
[82] D. Liu, K. Savino, M. Yates, C. Technology, Coating of hydroxyapatite films on metal substrates by seeded hydrothermal deposition, Surf, Coat. Technol. 205 (16) (2011) 3975–3986.